A bistable computational model of recurring epileptiform activity as observed in rodent slice preparations

Robert D. Vincent[a,*], Aaron Courville[b], Joelle Pineau[a]

[a] *McGill University, School of Computer Science, 3480 University Street, Montreal, Quebec H3A 2A7, Canada*
[b] *Département d'informatique et de Recherche Opérationelle, Université de Montréal, Montreal, Quebec, Canada*

Abstract

We describe a computational model of epileptiform activity mimicking the activity exhibited by an animal model of epilepsy *in vitro*. The computational model permits generation of synthetic data to assist in the evaluation of new algorithms for epilepsy treatment via adaptive neurostimulation. The model implements both single-compartment pyramidal neurons and fast-spiking interneurons, arranged in a one-dimensional network using both excitatory and inhibitory synapses. The model tracks changes in extracellular ion concentrations, which determine the reversal potentials of membrane currents. Changes in simulated ion concentration provide positive feedback which drives the system towards the epileptiform state. One mechanism of positive feedback explored by this model is the conversion of pyramidal cells from regular spiking to intrinsic bursting as extracellular potassium concentration increases. One of the main contributions of this work is the development of a slow depression mechanism that enforces seizure termination. The network spontaneously leaves the seizure-like state as the slow depression variable decreases. This is one of the first detailed computational models of epileptiform activity which exhibits realistic transitions between inter-seizure and seizure states, and back, with state durations similar to the *in vitro* model. We validate the computational model by comparing its state durations to those of the biological model. We also show that electrical stimulation of the computational model achieves seizure suppression comparable to that observed in the *in vitro* model.

Keywords: epilepsy, computational models, deep brain stimulation

1. Introduction

Implanted electrical stimulation devices have emerged as a means to alleviate seizures (also known as *ictal* discharges or events) in patients with refractory epilepsy (Uthman et al., 2004). A recent development is the design of responsive stimulation algorithms which apply electrical stimulation only when it is most useful (Sun et al., 2008). Many of the methods being considered for the design of these dynamic or adaptive strategies require a large quantity of data to support both the design and validation of potential responsive stimulation algorithms (Guez et al., 2008; Bush & Pineau, 2009). Models of epilepsy, whether biological or computational, are a potential source of data for either designing or evaluating these algorithms.

In vitro models of epilepsy using rodent brain slice preparations provide a means to study the disease in a relatively consistent manner. They involve a significant reduction in the size and complexity of the neural circuits compared to the intact brain, while maintaining most of the key electrographic features of epilepsy seen *in vivo*. One common acute *in vitro* model of epilepsy is the 4-aminopyridine (4-AP) model. Brain slices treated with micromolar concentrations of 4-AP exhibit epileptiform activity consisting of events analogous to both ictal discharges and interictal spikes [1]. These ictal events may last for several tens of seconds, with interictal periods of several minutes, repeating over a period of several hours.

While *in vitro* models of epilepsy are useful for research, they nonetheless require large investments in training, equipment, and animal care. In contrast, computational models can provide large amounts of data for

*Corresponding author
Email address: bert@cs.mcgill.ca (Robert D. Vincent)

[1] An *ictal discharge* or *ictal event* is an electrographic anomaly lasting several seconds or more (and is often called a *seizure*), whereas an *interictal discharge* or *interictal spike* is typically a brief event lasting less than a second.

little cost. Experiments on computational models are, by nature, perfectly reproducible, and may permit precise manipulations which may be difficult or impossible in a biological model.

To generate useful synthetic data, a computational model of epilepsy must mimic key characteristics of the corresponding biological system. One important characteristic is the timing and duration of the epileptiform events, because this likely reflects fundamental properties of the epileptic network. However, prior computational models do not exhibit spontaneous transitions between epileptiform and normal states (Netoff et al., 2004; Bazhenov et al., 2004; Cressman et al., 2009; Ullah et al., 2009; Fröhlich et al., 2010), or they exhibit only brief events that resemble interictal spikes (Traub et al., 1995, 2001; Franaszczuk et al., 2003). Alternatively, many existing computational models are either too abstract (Biswal & Dasgupta, 2002; Ohayon et al., 2004; Suffczynski et al., 2004) or too computationally demanding (Traub et al., 2005) to permit the kinds of investigations needed for responsive stimulation algorithms.

In this paper, we present a computational model of epileptiform behavior in brain slices treated with 4-AP *in vitro* (Avoli et al., 2002). The primary goal of this research is the creation of a computational model of epilepsy that generates data which can be used to develop and test dynamic electrical stimulation algorithms for seizure suppression.

This model builds on prior work on bursting behavior in low-magnesium preparations (Golomb et al., 2006), using a simple single-compartment model for cortical pyramidal cells and fast-spiking inhibitory interneurons. Instead of a using a mean-field approximation for modeling synaptic currents, we use an explicit model of individual synapses (Destexhe et al., 1998).

We further extend this prior work by incorporating a model of changes in extracellular ion (Na^+, K^+) concentration before and during seizures (Heinemann et al., 1977; Kager et al., 2000). These ion concentration changes may be an important contributor to the initiation and maintenance of ictal behavior (Fröhlich et al., 2008).

Less well understood, however, are the mechanisms which account for seizure termination (Löscher & Köhling, 2010). Our model incorporates a slow, activity-dependent reduction in synaptic efficiency, which accounts for the transition from seizure to non-seizure states. While this mechanism is too simple to enable a direct comparison, this slow depression mechanism follows a time course similar to the observed relationship between seizure termination and intracellular or extracellular acidosis (Xiong et al., 2000; Ziemann et al., 2008).

Given the goal of providing simulated data for adaptive stimulation experiments, the computational model must respond to electrical stimulation in a realistic manner. We are particularly concerned with the effects of fixed-frequency stimulation or "periodic pacing" in the 0.5-1 Hz range. Stimulation in this frequency range has been shown consistently to reduce or suppress ictal events *in vitro* (D'Arcangelo et al., 2005; Durand & Bikson, 2001). We demonstrate that our model responds to a simulated electrode input from a stimulation device with a reduction in duration and frequency of seizure-like events that is similar to that observed in *in vitro* models.

The primary contribution of this paper is to propose a bistable network that roughly matches the observed statistical distribution of ictal/interictal phases in the 4-AP *in vitro* model. We show that our computational model can spontaneously transition between the ictal and interictal states, over simulations covering several tens of minutes. The model is computationally efficient and can generate data for many hundreds of seconds of simulated time. We also make the model available for the use of other researchers[2].

2. Methods

A set of six examples of biological data were acquired using rat brain slices *in vitro*, using the protocol detailed in this section. These data were then compared with the results observed in the computational model, which combines elements from several previously published models, as described below.

2.1. In vitro data collection

Male, adult Sprague-Dawley rats (250-300 g) were decapitated under deep isoflurane anesthesia. The brain was quickly removed and placed in cold ($0 - 2^\circ$ C) artificial cerebrospinal fluid (aCSF), having the following composition (mM): 124 NaCl, 2 KCl, 2 $MgSO_4$, 2 $CaCl_2$, 1.25 KH_2-PO_4, 26 $NaHCO_3$ and 10 D-glucose, continuously bubbled with gas mixture (O_2 95% and CO_2 5%) to equilibrate at pH~7.40. Combined hippocampus-entorhinal cortex (EC) slices 450 μm thick were cut as previously described (D'Arcangelo et al., 2005) using a VT1000S vibratome (Leica, Germany). Slices were then transferred to an interface

[2]Source code may be downloaded at `http://www.cs.mcgill.ca/~rvince3/ivmodel.tar.gz`

recording chamber, lying between warm (∼ 32° C) aCSF and humidified gas (O_2 95% and CO_2 5%), where they were allowed to recover for at least one hour before beginning continuous bath application (1 ml/min) of 4-aminopyridine (4-AP). 4-AP is a potassium (K^+) channel blocker which increases neuronal excitability (Perreault & Avoli, 1991). Consequently, continuous perfusion of brain slices with micromolar concentrations of 4-AP leads to the generation of spontaneous epileptiform discharges resembling electrographic seizures and interictal spikes. We analyzed six slices obtained from six animals. All of the procedures were carried on in accordance to the CCAC (Canadian Council for Animal Care) and McGill University guidelines.

Field potential recording was performed with aCSF-filled pipettes (tip diameter < 10 μm; resistance= 5-10 MΩ) pulled from borosilicate capillary tubing (World Precision Instruments Inc., Sarasota, FL, USA) using a P-97 puller (Sutter Instrument, Novato, CA, USA). Extracellular signals were fed to a Cyberamp 380 amplifier (Molecular Devices, Palo Alto, CA) connected to a digital interface device (Digidata 1322A, Molecular Devices). Data were acquired at a sampling rate of 5 kHz, using the software Clampex 8.2 (Molecular Devices), stored on the hard drive and analyzed offline. Recording electrodes were placed in the deep layers of the medial EC. Extracellular current pulses (100-250 μA, pulse width 100 μsec) were delivered in the subiculum through a bipolar concentric Pt-Ir electrode (FHC, Bowdoin, ME, USA) plugged into a high voltage stimulus isolator unit (A360, WPI Inc., Sarasota, Florida, USA) connected to the pulse generator Pulsemaster A300 (WPI Inc., Sarasota, Florida, USA).

An input/output curve was generated to adjust the stimulus intensity to reliably obtain an interictal-like event in the EC. The apparatus parameters were then fixed and the periodic pacing protocols at 0.5 Hz and 1.0 Hz were implemented. Each stimulation phase proceeded until at least 4 consecutive ictal-like discharges were observed (control) or until at least three times the previously observed interval between consecutive ictal-like discharges (stimulation) had elapsed. Each stimulation phase was immediately preceded by a control period and followed by a post-stimulation recovery period, which served as the control recording for the following stimulation protocol. Ictal discharge onset and termination were labeled in-house via visual inspection.

2.2. Computational model

To investigate the effects of extracellular ion concentrations on neuronal network dynamics, we used model neurons which extend standard Hodgkin-Huxley kinetics (Hodgkin & Huxley, 1952). The membrane current I_x associated with an arbitrary ion channel x is determined by equations of the general form:

$$I_x = \bar{g}_x r(V_m - E_x), \tag{1}$$

where $\bar{g}_x$ is the maximal conductance of the ion channel, V_m is the membrane potential, E_x is the equilibrium potential of the ion, and r is a gating variable which describes the fraction of gates which are in the open state.

A typical gating variable r follows a differential equation of the form:

$$\frac{dr}{dt} = \phi \frac{r_\infty - r}{\tau_r}, \tag{2}$$

where r_∞ and τ_r are the equilibrium value and time constants of the gate, respectively. Both of these are often functions of the membrane potential, V_m. The rate is modulated by the temperature correction factor, ϕ.

In some cases, the values of r_∞ and τ_r may be expressed as a function of a forward rate constant α_r and backward rate constant β_r:

$$r_\infty = \frac{\alpha_r}{\alpha_r + \beta_r} \tag{3}$$

and

$$\tau_r = \frac{1}{\alpha_r + \beta_r}. \tag{4}$$

In this case, Equation 2 may be rewritten as:

$$\frac{dr}{dt} = \phi(\alpha_r(1 - r) - \beta_r r). \tag{5}$$

The forward rate constant α_r represents the rate at which the gate is transitioning to an open state, whereas β_r represents the rate of conversion to a closed state. Both values are often functions of the membrane potential V_m, although they may also depend on other factors, such as extracellular ion concentrations.

2.2.1. Excitatory cell model

The excitatory cell model is a single-compartment pyramidal cell model that is relatively simple but which can be tuned to either a regular spiking (RS) mode or to an intrinsic bursting (IB) mode with only a small parameter change (Golomb & Amitai, 1997; Golomb et al., 2006). This enables the computational model to reflect the observed tendency for some neurons to transition from RS to IB mode in the presence of elevated K^+ (Jensen et al., 1994). This behavior is illustrated in Figure 1. This change manifests itself both as a change

in both the pattern and the average rate of firing. The effect on the mean rate is illustrated in Figure 2 B. These effects should tend to increase the probability of the firing of the postsynaptic neurons in response to the firing of a presynaptic neuron.

The membrane potential V_m is governed by the current balance equation

$$C\frac{dV_m}{dt} = -I_{\mathrm{Na}} - I_{\mathrm{NaP}} - I_{\mathrm{Kdr}} - I_{\mathrm{Kslow}} - I_{leak} - I_{syn} + I_{app}, \quad (6)$$

where $C = 1\ \mu\mathrm{F/cm}^2$ is the specific capacitance of the membrane. In addition to the applied (electrode) current I_{app} and synaptic current I_{syn}, the model includes five ion currents: the fast sodium current I_{Na}, the persistent sodium current I_{NaP}, the delayed-rectifier potassium current I_{Kdr}, the slow potassium current I_{Kslow}, and a leak current I_{leak} (Golomb & Amitai, 1997; Golomb et al., 2006).

For the fast Na^+ current I_{Na}, the activation is assumed to be instantaneous, so the current is given by:

$$I_{\mathrm{Na}} = \bar{g}_{\mathrm{Na}} m_\infty^3 h (V_m - E_{\mathrm{Na}}), \quad (7)$$

where

$$m_\infty = \frac{1}{1 + \exp\left(\frac{-(V_m - \theta_m)}{\sigma_m}\right)}, \quad (8)$$

$$h_\infty = \frac{1}{1 + \exp\left(\frac{-(V_m - \theta_h)}{\sigma_h}\right)} \quad (9)$$

$$\tau_h = 1 + \frac{7.5}{1 + \exp\left(\frac{-(V_m - \theta_{th})}{\sigma_{th}}\right)}, \quad (10)$$

where E_{Na} is the calculated reversal potential of Na^+, and m and h are the activation and inactivation variables (i.e. fraction of open channels). The constants are given in Table 1. The relationship between the inactivation variable h, τ_h, and h_∞ is given by Equation 2, with the temperature correction factor $\phi = 10$ at the simulation temperature of 37° (Golomb et al., 2006).

The persistent Na^+ current, I_{NaP}, is a non-inactivating current. It plays a critical role in the generation of intrinsic bursting behavior (Golomb et al., 2006), so it is of particular interest in our model. Again, the activation of this current is assumed to be instantaneous, and so it follows the equations:

$$I_{\mathrm{NaP}} = \bar{g}_{\mathrm{NaP}} p_\infty (V_m - E_{\mathrm{Na}}), \quad (11)$$

where the activation variable p is given by

$$p_\infty = \frac{1}{1 + \exp\left(\frac{-(V_m - \theta_p)}{\sigma_p}\right)}, \quad (12)$$

where p is the activation of the channel. All other constants are given in Table 1.

The delayed-rectifier K^+ current, I_{Kdr}, is also a non-inactivating current, obeying the following equations:

$$I_{\mathrm{Kdr}} = \bar{g}_{\mathrm{Kdr}} n^4 (V_m - E_{\mathrm{K}}), \quad (13)$$

where

$$n_\infty = \frac{1}{1 + \exp\left(\frac{-(V_m - \theta_n)}{\sigma_n}\right)} \quad (14)$$

$$\tau_n = 1 + \frac{5}{1 + \exp\left(\frac{-(V - \theta_m)}{\sigma_m}\right)}, \quad (15)$$

where n is the activation of the channel, E_{K} is the calculated reversal potential of K^+. Again, all constants are given in Table 1.

The slow K^+ current, I_{Kslow}, is also a non-inactivating current. It represents the collective effects of potassium currents with time constants in the tens or hundreds of milliseconds, those which typically are responsible for spike rate adaptation in regular spiking cells (Golomb et al., 2006). The kinetics are as follows:

$$I_{\mathrm{Kslow}} = \bar{g}_{\mathrm{Kslow}} z (V_m - E_{\mathrm{K}}), \quad (16)$$

where

$$z_\infty = \frac{1}{1 + \exp\left(\frac{-(V_m - \theta_z)}{\sigma_z}\right)}, \quad (17)$$

$$\tau_z = 75, \quad (18)$$

where z is the activation of the channel; constants are specified in Table 1.

Finally, the leak current I_{leak} is simply:

$$I_{leak} = g_{leak} (V_m - E_{leak}), \quad (19)$$

where E_{leak}, the reversal potential of the leak current, is calculated from the ion concentrations.

The synaptic current I_{syn} is the sum of three individual synaptic currents:

$$I_{syn} = I_{\mathrm{NMDA}} + I_{\mathrm{AMPA}} + I_{\mathrm{GABA_A}}, \quad (20)$$

these are further described in Section 2.2.3.

2.2.2. Inhibitory cell model

We model inhibitory cells using the Wang-Buzsáki model of fast-spiking (FS) interneurons (Wang & Buzsáki, 1996). The membrane potential V_m is given by the current balance equation:

$$C\frac{dV_m}{dt} = -I_{\mathrm{Na}(i)} - I_{\mathrm{Kdr}(i)} - I_{leak(i)} - I_{syn} + I_{app}. \quad (21)$$

Table 1: Constants for the model excitatory cell, taken directly from Golomb et al. (2006).

Symbol	Value	Units
θ_m	-30	mV
σ_m	9.5	mV
θ_h	-45	mV
σ_h	-7	mV
θ_{th}	-40.5	mV
σ_{th}	-6	mV
θ_p	-47	mV
σ_p	3	mV
θ_n	-33	mV
σ_n	10	mV
θ_{tn}	-27	mV
σ_{tn}	-15	mV
θ_z	-39	mV
σ_z	5	mV
$\bar{g}_{\mathrm{Na}}$	35	mS/cm^2
$\bar{g}_{\mathrm{NaP}}$	0.06	mS/cm^2
$\bar{g}_{\mathrm{Kdr}}$	6	mS/cm^2
$\bar{g}_{\mathrm{Kslow}}$	1.8	mS/cm^2
g_{leak}	0.05	mS/cm^2

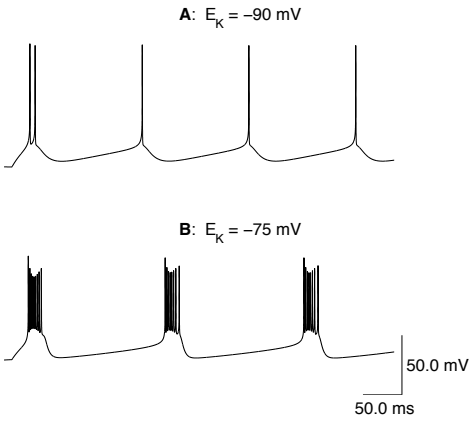

Figure 1: The pyramidal cell model proposed by Golomb and Amitai undergoes a mode change as $[\mathrm{K}^+]_\mathrm{o}$ increases and the potassium reversal potential depolarizes. Parameters are $\bar{g}_{\mathrm{NaP}} = 0.06$ mS/cm^2, $I_{app} = 1$ nA/cm^2. **A**: Regular spiking mode exhibited when the potassium reversal potential $E_\mathrm{K} = -90$ mV, the resting value. **B**: The model has transitioned to intrinsic bursting mode when $E_\mathrm{K} = -75$ mV.

Table 2: Constants for the model inhibitory cell (Wang & Buzsáki, 1996).

Symbol	Value	Units
$\theta_{\alpha M}$	-35	mV
$\sigma_{\alpha M}$	10	mV
$\theta_{\beta M}$	-60	mV
$\sigma_{\beta M}$	18	mV
$\theta_{\alpha H}$	-58	mV
$\sigma_{\alpha H}$	20	mV
$\theta_{\beta H}$	-28	mV
$\sigma_{\beta H}$	10	mV
$\theta_{\alpha N}$	-34	mV
$\sigma_{\alpha N}$	10	mV
$\theta_{\beta N}$	-44	mV
$\sigma_{\beta N}$	80	mV
$\bar{g}_{\mathrm{Na}(i)}$	35	mS/cm^2
$\bar{g}_{\mathrm{Kdr}(i)}$	9	mS/cm^2
$g_{leak(i)}$	0.1	mS/cm^2

The inhibitory cell includes only three ion currents, the fast sodium $I_{\mathrm{Na}(i)}$, the delayed-rectifier potassium $I_{\mathrm{Kdr}(i)}$, and a leak current $I_{leak(i)}$.

As in the excitatory cell model, the activation variable M of the fast sodium current has instantaneous dynamics:

$$I_{\mathrm{Na}(i)} = \bar{g}_{\mathrm{Na}(i)} M_\infty^3 H (V_m - E_{\mathrm{Na}}), \tag{22}$$

where

$$\alpha_M = \frac{0.1(V_m - \theta_{\alpha M})}{1 - \exp\left(\frac{-(V_m - \theta_{\alpha M})}{\sigma_{\alpha M}}\right)}, \tag{23}$$

$$\beta_M = 4 \exp\left(\frac{-(V_m - \theta_{\beta M})}{\sigma_{\beta M}}\right), \tag{24}$$

$$\alpha_H = 0.07 \exp\left(\frac{-(V_m - \theta_{\alpha H})}{\sigma_{\alpha H}}\right), \tag{25}$$

$$\beta_H = \frac{1}{1 + \exp\left(\frac{-(V_m - \theta_{\beta H})}{\sigma_{\beta H}}\right)}, \tag{26}$$

where all constants are given in Table 2.

The value of M_∞ is derived from α_M and β_M using Equation 3. The relationship among the variables H, α_H, and β_H is given by Equation 5, with a temperature correction factor $\phi = 5$ at the simulation temperature of 37° C.

The delayed-rectifier potassium current is also similar to that of the excitatory cell:

$$I_{\mathrm{Kdr}(i)} = \bar{g}_{\mathrm{Kdr}(i)} N^4 (V_m - E_\mathrm{K}), \tag{27}$$

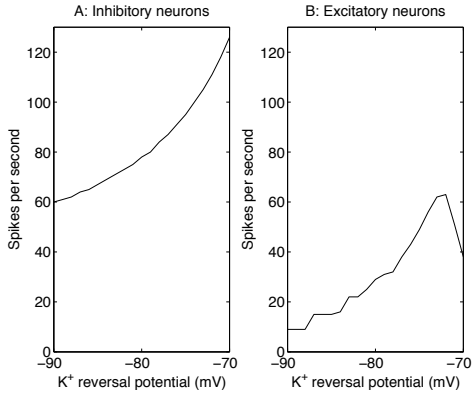

Figure 2: Spiking rates of the model neurons as a function of K^+ reversal potential. Applied current is 1 nA.

where

$$\alpha_N = \frac{0.01(V_m - \theta_{\alpha N})}{\left(1 - \exp\left(\frac{-(V_m - \theta_{\alpha N})}{\sigma_{\alpha N}}\right)\right)}, \quad (28)$$

$$\beta_N = 0.125 \exp\left(\frac{-(V_m - \theta_{\beta N})}{\sigma_{\beta N}}\right), \quad (29)$$

where all constants are given in Table 2. The reversal potentials E_{K} and E_{Na} are calculated from the ion concentrations as described in Section 2.2.5.

While the inhibitory model neuron does not exhibit a fundamental change in behavior similar to the excitatory cell's transition from RS to IB behavior, increasing the extracellular K^+ concentration does increase the spiking rate of the neuron (See Figure 2 A). This effect should provide negative feedback against the greater excitability of the pyramidal cells at high values of $[K^+]_o$.

2.2.3. Synaptic currents

All synaptic currents are calculated according to the simplified scheme described by Destexhe et al. (1998). Each current is controlled by a gating variable which represents the fraction of open channels in the synapse. As an example, the synaptic current I_{AMPA} has the form:

$$I_{\mathrm{AMPA}} = \bar{g}_{\mathrm{AMPA}} r (V_m - E_{\mathrm{AMPA}}), \quad (30)$$

where $\bar{g}_{\mathrm{AMPA}}$ is the maximal conductance of the synapse, E_{AMPA} is the reversal potential of the synapse (usually 0 mV), and r is the gating variable representing the fraction of open channels. In some cases, the gating variable may be further multiplied by additional factors which influence synaptic transmission. These factors may include, for example, either activity-dependent depression effects or phenomena such as the magnesium block of NMDA receptors (Jahr & Stevens, 1990).

Table 3: Rate constants for synaptic currents (Destexhe et al., 1998).

	α ($M^{-1}sec^{-1}$)	β (sec^{-1})
AMPA	1.1×10^6	190
NMDA	7.2×10^4	6.6
$GABA_A$	5×10^6	180

The gating variable, r, of a synaptic current is controlled by the differential equation:

$$\frac{dr}{dt} = \alpha[T](1 - r) - \beta r, \quad (31)$$

where $[T]$ is the concentration of neurotransmitter in the synaptic cleft and α and β are rate constant parameters chosen to fit observed synaptic activation time courses. For simplicity, the neurotransmitter concentration is modeled as a single 1 millisecond pulse with concentration 1 mM (Destexhe et al., 1998). The parameter values are given in Table 3. For computational efficiency, the synaptic state variables are associated with the presynaptic neuron. This choice is possible because the model neurons have a single compartment, therefore all synapses are triggered simultaneously.

The AMPA and $GABA_A$ receptor models are straightforward implementations of the simplified first-order model presented in Destexhe et al. (1998). There is evidence that increasing $[K^+]_o$ will decrease the driving force of the $GABA_A$ inhibitory effect by decreasing the efficiency of combined K^+/Cl^- transport (Jensen et al., 1993), and strong evidence that $GABA_A$ plays an important role in seizure initiation (Avoli et al., 2002). The details of these interactions remain an area of ongoing research (Rivera et al., 2004). However, modeling the complex interactions of this mechanism was not attempted in the current study, as few sufficiently detailed quantitative descriptions of these effects exist, and modeling concentrations of $Cl^-$and Ca^{2+}would significantly increase the computational requirements of the overall model.

The model NMDA receptor is modified slightly from prior work to account for the effects of $[K^+]_o$ on the synaptic efficacy. The NMDA receptor is a slow-acting glutamatergic receptor, which has a well-known dependence on voltage and extracellular Mg^{2+} concentration (Jahr & Stevens, 1990). More relevant to the 4-AP model, there is evidence that elevated $[K^+]_o$ increases both glutamate release (Crowder et al., 1987; Fujikawa et al., 1996) and NMDA receptor activation (Poolos & Kocsis, 1990).

We use the following equation to calculate the synap-

tic current due to NMDA:

$$g_{\mathrm{NMDA}} = \bar{g}_{\mathrm{NMDA}} B(V_m, [\mathrm{Mg}^{2+}]_\mathrm{o}) G([\mathrm{K}^+]_\mathrm{o}) s \quad (32)$$

$$I_{\mathrm{NMDA}} = g_{\mathrm{NMDA}}(V_m - E_{\mathrm{NMDA}}), \quad (33)$$

where $\bar{g}_{\mathrm{NMDA}}$ is the maximal conductance of the NMDA receptor, s is the gating variable for NMDA, and $E_{\mathrm{NMDA}} = 0$ mV. The function B accounts for the voltage-dependent magnesium block associated with the NMDA receptor (Jahr & Stevens, 1990; Dayan & Abbott, 2001):

$$B(V_m, [\mathrm{Mg}^{2+}]_\mathrm{o}) = \frac{1}{1 + \frac{[\mathrm{Mg}^{2+}]_\mathrm{o}}{3.57} \exp\left(\frac{-V_m}{16.13}\right)}. \quad (34)$$

The enhancement of NMDA receptor activity by $[\mathrm{K}^+]_\mathrm{o}$ is given by the equation:

$$G([\mathrm{K}^+]_\mathrm{o}) = \frac{100.0}{1.0 + \exp(-\frac{[\mathrm{K}^+]_\mathrm{o} - 11.75}{1.7974})}. \quad (35)$$

This equation and constants were chosen to approximate the behavior modeled by Kager et al. (2000).

In addition, the excitatory-excitatory synaptic currents (whether AMPA or NMDA) are moderated by two different forms of synaptic depression, one fast (D) and another slow (Q).

The fast depression variable is a phenomenological reflection of the decrease in the availability of "synaptic resources" after firing (Abbott et al., 1997; Bazhenov et al., 2004). When a neuron i fires, the value of D is instantaneously replaced according to the equation:

$$D^i_{t+1} = D^i_t(1 - \Delta_D), \quad (36)$$

and recovers according to the differential equation:

$$\frac{dD^i}{dt} = \frac{(1 - D^i)}{\tau_D}, \quad (37)$$

where $\Delta_D = 0.07$ is the fraction of synaptic resources used per firing, D^i_t is the depression factor of the ith neuron at time t, and $\tau_D = 0.7$ sec is the recovery time.

The slow depression follows the same algorithm as fast depression, but on a much longer time scale and with a slower recovery rate. It is meant to model slower phenomena that provide negative feedback and seizure termination. It has an identical form as that for the fast depression D:

$$Q^i_{t+1} = Q^i_t(1 - \Delta_Q), \quad (38)$$

and

$$\frac{dQ^i}{dt} = \frac{(1 - Q^i)}{\tau_Q}, \quad (39)$$

where Δ_Q is the fractional decrease in Q per firing, and τ_Q is the recovery time constant. This slower effect is intended to be consistent with possible mechanisms of seizure termination, such as activity-dependent acidosis (Xiong et al., 2000; Ziemann et al., 2008), for example.

The factors D and Q act to reduce the synaptic conductance in excitatory-excitatory synapses (either AMPA or NMDA). For example, for an AMPA synapse from presynaptic pyramidal cell i to postsynaptic pyramidal cell j, the full equation for the synaptic current is:

$$I^j_{\mathrm{AMPA}} = \bar{g}_{\mathrm{AMPA}} r^i D^i Q^i (V^j_m - E_{\mathrm{AMPA}}). \quad (40)$$

2.2.4. Ion concentrations

We model the changes in the extracellular ion concentrations of both Na^+ and K^+ following the formalism introduced by Kager et al. (2000).

Changes in intracellular and extracellular ion concentrations are modeled by integrating the appropriate currents over time and converting to concentration units. Therefore the change in intracellular concentration for an ion is given by:

$$\frac{d[\mathrm{Ion}]_i}{dt} = \frac{A \sum_{\mathrm{Ion}} I_{Ion}}{F V_i}, \quad (41)$$

where A is the surface area of the membrane, F is the Faraday constant, and V_i is the intracellular volume. The corresponding change in extracellular concentration is given by:

$$\frac{d[\mathrm{Ion}]_o}{dt} = -\frac{A \sum_{\mathrm{Ion}} I_{Ion}}{F V_o}, \quad (42)$$

where V_o is the volume of the extracellular space around the cell, here estimated to be $0.15 V_i$ (Kager et al., 2000).

Ion concentrations are restored primarily through the action of an active "ion pump" model which responds to elevated extracellular K^+ and intracellular Na^+ (Läuger, 1991; Kager et al., 2000).

The pump activation is given by:

$$A_{pump} = \left(1 + \frac{[\mathrm{K}^+]_{\mathrm{o(eq)}}}{[\mathrm{K}^+]_\mathrm{o}}\right)^{-2} \left(1 + \frac{[\mathrm{Na}^+]_{\mathrm{i(eq)}}}{[\mathrm{Na}^+]_i}\right)^{-3}, \quad (43)$$

where $[\mathrm{K}^+]_{\mathrm{o(eq)}} = 3.5$ mM and $[\mathrm{Na}^+]_{\mathrm{i(eq)}} = 10$ mM are the equilibrium values for extracellular potassium and intracellular sodium (Kager et al., 2000).

Because the pump exchanges 2 K^+ for 3 Na^+, the current from the pump is given by:

$$I_{Kpump} = -2 I_{max} A_{pump} \quad (44)$$

$$I_{Napump} = 3 I_{max} A_{pump}, \quad (45)$$

where the value of I_{max} is chosen to balance the ion flux at equilibrium.

The model of the extracellular space includes a model of glial uptake (Kager et al., 2000) and diffusion between compartments (Bazhenov et al., 2004). The glial buffering system assumes a fixed reverse rate constant $k_1 = 0.015$[3] and a forward rate constant k_2 that depends on $[K^+]_o$ (Kager et al., 2000):

$$k_2 = \frac{k_1}{1 + \exp\left(\frac{[K^+]_o - 15}{-1.09}\right)}. \quad (46)$$

Diffusion is assumed to occur only between adjacent extracellular compartments. The resulting differential equation for $[K^+]_o$ is:

$$\frac{d[K^+]_o}{dt} = \frac{kI_K^\Sigma}{Fd} + G + \frac{\mathcal{D}}{\Delta x^2}([K^+]_{o(+)} + [K^+]_{o(-)} - 2[K^+]_o), \quad (47)$$

where F is the Faraday constant, $k = 10$ is a unit conversion constant (needed to convert the result into units of mM/sec), $d = 0.15$ μm is the ratio of the extracellular volume to the surface area, and I_K^Σ is the sum of all K^+ currents, including the inward pump. The constant $\mathcal{D} = 2 \times 10^{-6}$ cm^2/s is the diffusion coefficient and $\Delta x = 100$ μm is the distance between adjacent neurons. $[K^+]_{o(+)}$ and $[K^+]_{o(-)}$ are the extracellular K^+ concentrations of adjacent cells in the one-dimensional array (Bazhenov et al., 2004).

The variable G represents the kinetics of the glial buffering model. It is described by the equations:

$$G = k_1 \frac{([B]_{max} - [B])}{k_{1N}} - k_2[K^+]_o[B] \quad (48)$$

$$\frac{d[B]}{dt} = k_1([B]_{max} - [B]) - k_2[K^+]_o[B], \quad (49)$$

where [B] is the free buffer concentration, $[B]_{max} = 500$ mM is the maximum buffering capacity of the glial cells, and $k_{1N} = 1.1$ (Bazhenov et al., 2004).

While there is debate about the importance of these ion concentration effects, it seems reasonable to conclude that they may be a source of positive feedback that either helps initiate or sustain ictal events (Kager et al., 2000; Bazhenov et al., 2004; Fröhlich et al., 2008).

To account for other unknown mechanisms of homeostasis of the relevant ion concentrations, and to maintain stability over the long simulation periods used in this study, we introduced an additional exponential decay towards the equilibrium values for both intracellular and extracellular K^+ and Na^+ concentrations. This decay is intentionally fairly slow, with a time constant of two seconds.

[3]This value gives substantially faster rates than used in Kager et al. (2000).

2.2.5. Reversal potentials

In biological networks, the Na^+ and K^+ reversal potentials, E_{Na} and E_K depend on the relative concentration of relevant ions in the intracellular and extracellular space. This dependency is most simply expressed using the Nernst equation:

$$E = \frac{RT}{zF} \ln \frac{[ion]_o}{[ion]_i}, \quad (50)$$

where R is the ideal gas constant, T is the temperature in Kelvin, F is the Faraday constant, z charge of the ion, and $[ion]_o$ and $[ion]_i$ are the extracellular and intracellular concentrations of the ion.

Many prior computational models assume a constant value for the reversal potential. While a reasonable approximation for models of normal activity, the assumption of constant reversal potentials is not realistic in the case of epileptiform activity, given the evidence for large changes in concentration of, for example, extracellular K^+ ions observed during ictal events *in vitro* (Heinemann et al., 1977; Avoli et al., 2002).

2.2.6. Electrical stimulation

Electrical stimulation I_{app} is modeled as a direct input to two of the excitatory cells in the simulation. The current applied in most experiments was 0.4 nA, each pulse having a duration of 40 msec.

2.2.7. Network structure

Evidence suggests that epileptiform activity in the *in vitro* slice model may initiate within layer V of the entorhinal cortex (Avoli et al., 2002), therefore we attempt to model a single layer of cortical cells without additional sources of complexity or feedback.

The network is arranged in a simple linear structure of 32 units. Larger networks (on the order of 100 units) were used in some simulations, with comparable results. However, the computation time required for larger networks renders them impractical for long simulations.

Each neuron synapses onto its ten nearest neighbors. Every fourth neuron is inhibitory, giving an overall 3:1 ratio between excitatory and inhibitory neurons.

2.2.8. Background activity

In order to simulate the intrinsic background level of activity in the network, each model neuron is driven by a Poisson-distributed sequence of random firing events.

That is, each model neuron has a small probability of firing spontaneously during each time step. In most of the simulations presented below, this firing rate was set such that each neuron fires on average once every 50 seconds. This choice is somewhat arbitrary, but in early experiments the model was found to give similar results over a fairly wide range of values for the average firing rate.

2.2.9. Implementation

The software is implemented in the C programming language. Numeric integration is performed using a 4th-order Runge-Kutta method with a time step of 0.01 milliseconds, with the exception of the synaptic conductances, which are integrated using the method proposed in Destexhe et al. (1998). On a 3.0 GHz Intel Xeon processor, the code requires about ten hours of real time to calculate the state of the model over 1200 seconds of simulated time. Source code for the model can be downloaded at the URL: `http://www.cs.mcgill.ca/~rvince3/ivmodel.tar.gz`.

3. Results

We now describe the observations made using the computational model, and compare these observations with the results of experiments performed *in vitro*. It is worth emphasizing that we use the data from the biological experiments only for comparison, not to directly fit the parameters of the model.

3.1. Typical behavior of the computational model

We examined the behavior of the computational model and visually compared it with typical behavior of the *in vitro* slice model.

Figure 3, panel B shows the behavior of the computational model compared to epileptiform activity generated by a brain slice treated with 4-AP (panel A). Note that the y axis for the biological model in Figure 3 represents the measured extracellular field potential, whereas for the computational model, the y axis is the simulated field potential, calculated as described in Tateno, Hayashi & Ishizuka (1998).

The duration of seizure-like states and the inter-seizure intervals are qualitatively similar in this example. In addition, both models show some interictal activity, although the interictal noise level in the computational model is lower. The computational model also shows a fairly clear preictal phase, with increasing brief bursts of activity which precede the sustained ictal-like event. The distribution of interictal bursts in the biological model is somewhat less orderly, but shows a similar increase in frequency leading up to the ictal phase.

Table 4: Comparison of mean seizure duration (SD) and inter-seizure interval (ISI) for the computational and *in vitro* models ($\Delta_Q = 0.00042$ and $\tau_Q = 160$).

	Mean SD	Mean ISI
In vitro model	81±18 sec	369±105 sec
Computational model	80±5 sec	357±38 sec

Figure 4 shows additional detail of the first ictal-like event generated by the computational model (Figure 3 B). The raster plot (Figure 4 A) shows the detailed firing pattern of all of the neurons in the network, including the detailed firing pattern during five seconds of ictal-like activity. The activity is characterized by hypersynchronous firing at approximately 3 Hz.

3.2. Comparison of the distribution of state durations

To quantitatively validate the model, we compared the distribution of simulated seizure durations and inter-seizure intervals (ISI) to that observed *in vitro*. The inter-seizure interval is defined as the time elapsed from the onset of a particular seizure to the onset of the next seizure.

Data obtained from *in vitro* recordings were manually labeled, whereas for the computational model, the event durations were determined from a trace representing one hour of simulated time with $\Delta_Q = 0.00042$ and $\tau_Q = 160$ seconds. These parameter values were chosen from a range of values observed to give event timings similar to those observed *in vitro*. Ictal phases were automatically identified using an algorithmic criterion. The onset of an ictal event is declared when more than 20 units have fired within 8 consecutive 10-msec windows. The ictal event is deemed to have terminated when fewer than 10 units fire for 40 consecutive 10-msec windows.

As shown in Table 4, simulated seizure-like events have a mean duration similar to those observed *in vitro*. The computational model clearly exhibits less variance than is present in the biological data, but the agreement is nevertheless quite good. The estimates for the biological data is derived from the mean seizure duration and inter-seizure interval for six experiments using different animals, so the difference in variance is unsurprising.

3.3. Extracellular potassium concentration

It has long been established that extracellular potassium concentration increases substantially, by as much

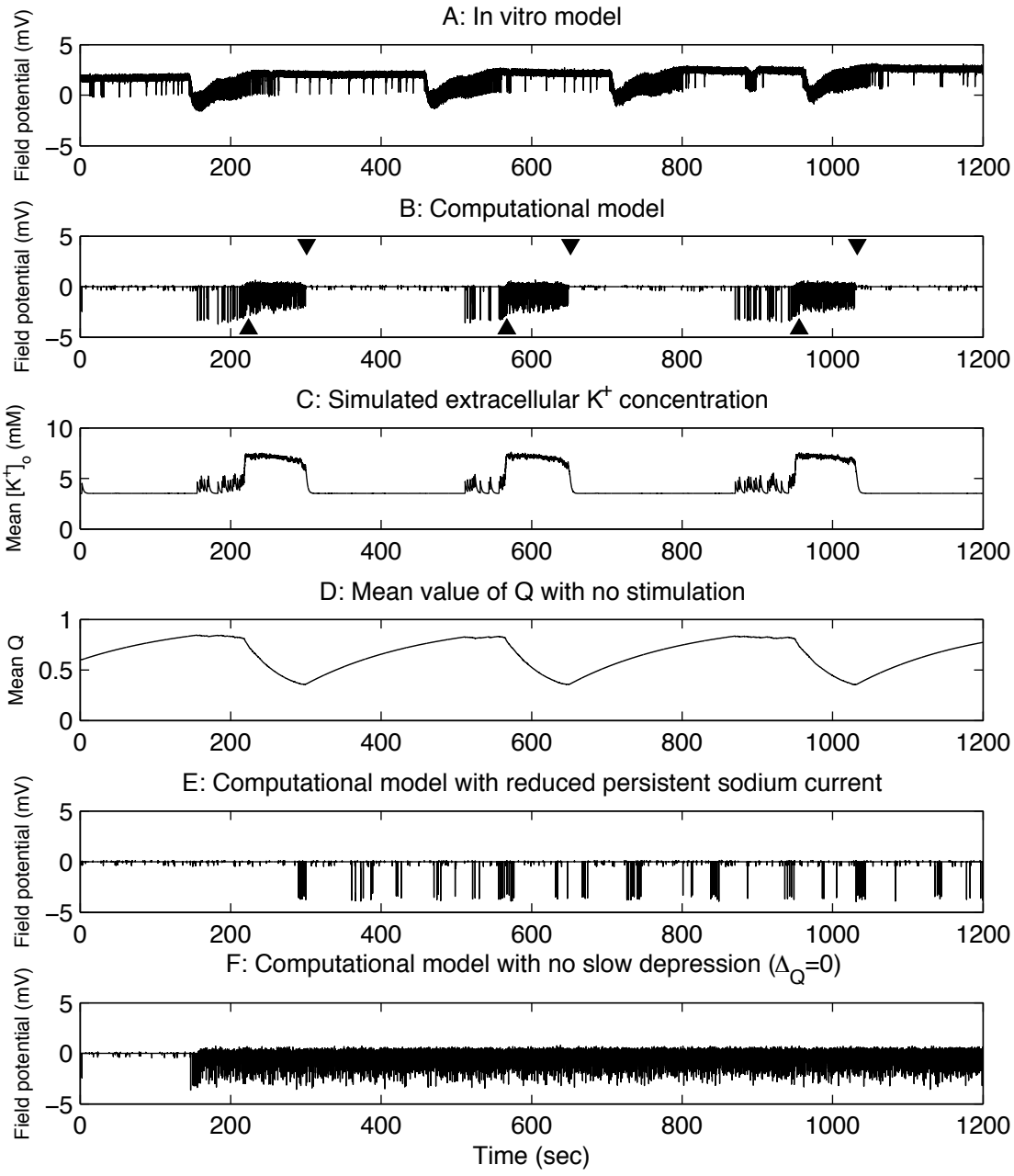

Figure 3: A: Example traces generated by the *in vitro* 4-AP biological model; B: The computational model (upward-pointing arrowheads indicate automatically calculated points of seizure onset, downward-pointing arrows indicate seizure termination); C: The mean extracellular potassium concentration of the computational model; D: The mean value of the slow depression variable Q over the same simulation period, with no stimulation and $\Delta_Q = 0.00042$, $\tau_Q = 160$. E: The computational model with reduced $\bar{g}_{\mathrm{NaP}}$; F: The computational model with $\Delta_Q = 0$, i.e. no slow depression;

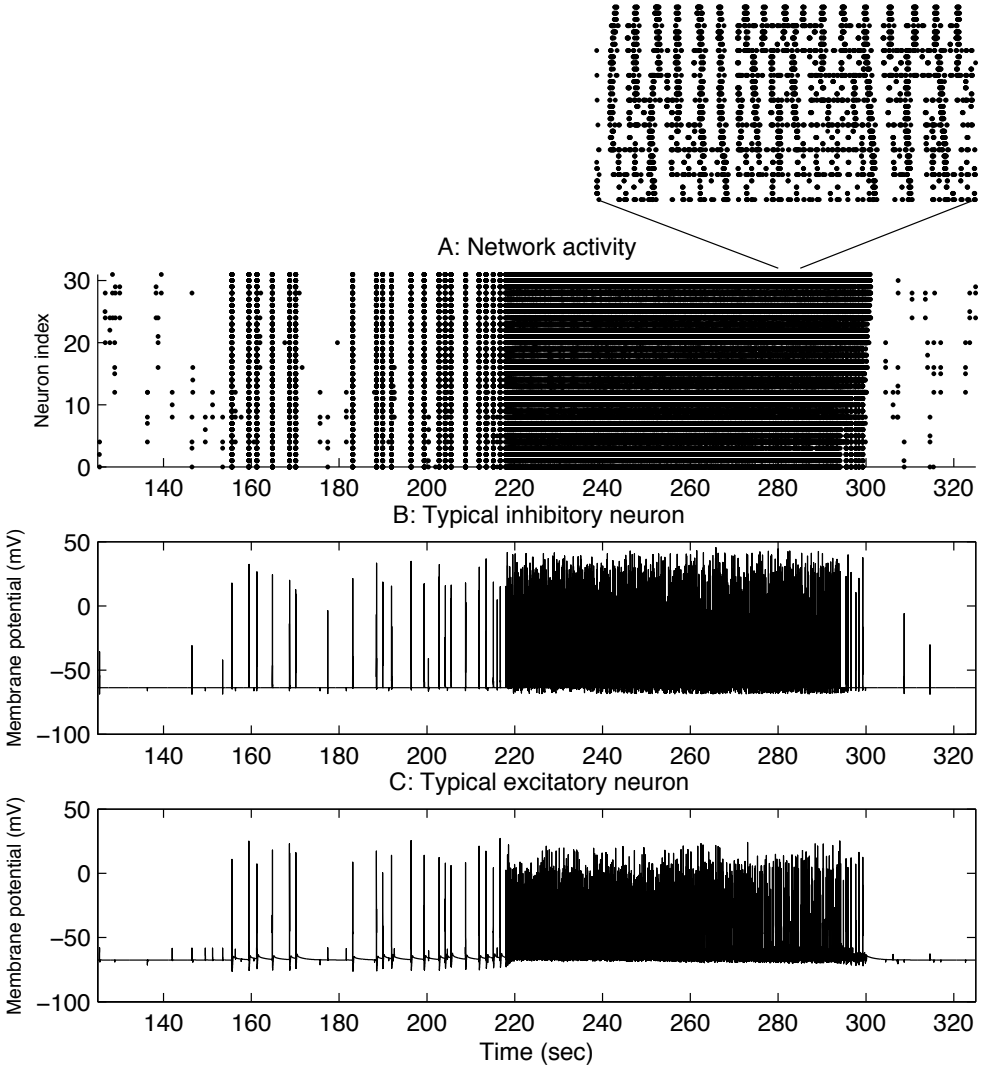

Figure 4: Detail of activity in the computational model during the first ictal-like event depicted in Figure 3 B. A: The raster plot shows the firing times of all units in the network (the inset shows additional detail for a typical five second interval of ictal-like activity); B: Membrane potential for one simulated inhibitory neuron; C: Membrane potential for one simulated excitatory neuron.

as 400%, during seizure-like events *in vitro* (Heinemann et al., 1977; Avoli et al., 2002). This fact has contributed to speculation that extracellular potassium plays an important role in either initiating or sustaining seizure-like events.

The behavior of extracellular potassium in the computational model is illustrated in Figure 3, panel C. This trace corresponds to the mean $[K^+]_o$ value of the network during the same simulation period depicted in panel B. During seizure-like events, the mean value of $[K^+]_o$ increases to slightly more than twice the baseline (maximum value typically ~7.6 mM).

The observed increase in $[K^+]_o$ from 3.5 mM to 7.6 mM corresponds to a change in E_K, the K^+reversal potential, from -89 mV to -68 mV. This change is more than enough to cause the model pyramidal cells to transition from RS to IB modes, as illustrated in Figure 1.

The observed changes in extracellular potassium concentration in the computational model are consistent with the timing and magnitude of those previously reported in relevant biological models (Heinemann et al., 1977; Avoli et al., 2002). These values are also consistent with those reported in related computational models (Kager et al., 2000; Bazhenov et al., 2004). In all of these cases, the value of $[K^+]_o$ is observed to increase rapidly during the beginning of the ictal event, then to level off or even to decline before the network returns to the interictal state.

3.4. Effect of persistent sodium current

While research suggests that some cortical cells tend to transition from regular spiking to intrinsic bursting in the presence of elevated $[K^+]_o$ (Jensen et al., 1994), this phenomenon has not been widely examined computationally. It has been suggested (Su et al., 2001) that the persistent sodium current I_{NaP} may play an important role in the generation of intrinsic bursting. It is also known that the maximal conductance of this current mediates bursting behavior in the model pyramidal neuron (Golomb et al., 2006). To verify the importance of this mode change to the initiation and maintenance of ictal-like events, we recorded the behavior of the computational model with a reduced value for the maximal conductance, $\bar{g}_{NaP}$.

Reducing the maximal conductance of the persistent sodium current from 0.06 to 0.025 mS/cm^2 inhibits the transition from RS to IB. This completely eliminates the generation of ictal-like events in the model. Instead, the model exhibits only brief bursts of activity (Figure 3, panel E).

In the model pyramidal neuron, the persistent sodium current is an important enabler of the transition to bursting behavior, as illustrated in Figure 1. When this bursting behavior is blocked, the model is robbed of an important source of positive feedback, and epileptiform events are no longer possible.

3.5. Effect of slow depression on seizure termination

To verify the contribution of the slow, activity-dependent depression state variable Q to the termination of seizure-like events, we run experiments in which the decay parameter Δ_Q is set to zero. As can be seen in Figure 3, panel F, this causes the seizure-like events to continue indefinitely. The slow depression mechanism is clearly responsible for seizure termination in the computational model. When the mechanism is disabled, the model cannot transition from the seizure-like state to the non-seizure state.

Figure 3, panel D, shows the average value of the state variable Q throughout the same simulation depicted in panels B and C. The mean value of Q clearly tracks the state changes of the network. As the value increases towards a threshold (~0.8), the network becomes susceptible to an ictal event. During the ictal event, Q quickly decays. A minimum (~0.4) is reached as the event terminates, and the value begins to recover. While this mechanism does not specifically model the effects of acidification, this general pattern is quite consistent with the time course of intracellular acidification reported by Xiong et al. (2000)

The choice of the parameters Δ_Q and τ_Q affect the mean duration of seizure-like events and the inter-seizure interval. For example, choosing $\Delta_Q = 0.00024$ and $\tau_Q = 240$ produces a model with a mean seizure duration of 165 ± 7 seconds and a mean inter-seizure interval of 500 ± 21 seconds. These values are large, but not implausible, as the maximum seizure length recorded in the control condition in our biological data was 182 seconds.

3.6. Response to stimulation

We further validated the computational model by comparing the effects of electrical stimulation in the computational model to the effects observed in the *in vitro* data described in Section 2.1.

Electrical stimulation was applied to the computational model by setting I_{app} to 0.4 nA for 40 milliseconds, simulating a square monopolar pulse applied directly to the cell membrane. The pulses are applied at 0.5 or 1.0 Hz, and the effect on the slice's ability to transition to the ictal state is quantified by calculating the fraction of time spent in seizure for each stimulation frequency.

The seizure suppression observed in each model for each stimulation frequency shows is very similar over the reported frequencies. The results are summarized in Figure 5, comparing the fraction of time spent in the seizure state at a given stimulation frequency. The computational model exhibits 58% reduction of seizure-like events at 0.5 Hz, achieving complete suppression at 1.0 Hz. The biological model exhibits a mean 70% reduction in seizure-like events at 0.5 Hz, with a complete elimination of seizure-like events at 1.0 Hz.

Figure 6 illustrates the effect of 1.0 Hz stimulation on the model. While the stimulation leads to elevated $[K^+]_o$(Figure 6 B), which would ordinarily lead to an increase in excitability in the network. However, as seen in Figure 6 C, the stimulation also forces the activity-dependent slow depression variable into a near steady-state value well below that which typically precedes ictal events. The resulting reduction in synaptic efficiency is apparently sufficient to counterbalance the effects of slightly increased $[K^+]_o$.

4. Discussion

The computational model presented above shows many similarities to the 4-AP *in vitro* animal model. Most important is the model's bistability, which is exhibited as spontaneous transitions from the interictal to ictal states, and subsequently returning to the interictal state. As with the biological model, these transitions occur with a fairly regular temporal pattern, and with fairly consistent durations of ictal and interictal states. We can control the timing of these phases by adjusting the parameters Δ_Q and τ_Q. The reduced variance in the timing of these phases is likely due to the relative homogeneity of the computational model, with identical parameters used for all model neurons and synapses.

Our model is able to mimic these statistics over realistic periods of simulated time, on the order of several tens of minutes, which allows us to measure the durations of several ictal and interictal states. However, longer simulation times impose severe restrictions on the complexity of some aspects of the model. This limits our ability to state with confidence that the computational model will reflect the response of the 4-AP model to novel stimulation patterns. Confirming this would require extensive electrophysiological work, as well as possibly mandating a more complete model of seizure initiation that includes the contributions of GABAergic receptors and the KCC2 K^+-Cl^- cotransporter (Avoli et al., 2002; Rivera et al., 2004).

Our computational model further demonstrates that a simple mechanism consisting of a slow activity-dependent decrease in synaptic transmission can account for the timing of seizure-like activity seen in the 4-AP model *in vitro*. This mechanism also provides an account for the effects of periodic pacing, as the continual excitation of the network serves to depress the efficiency of synaptic transmission. As a result, the synaptic efficiency cannot rise above the critical level required for the onset of ictal events.

It is not clear how closely our proposed seizure termination mechanism reflects the underlying biology. There is good agreement between the biological and computational data observed. However, this remains an understudied area. A reduction in synaptic efficiency is just one of several possible mechanisms which could reduce the runaway propagation of activity in a network. It is likely that many alternative mechanisms (e.g. hyperpolarization of the cell membrane, relative changes in ion channel conductivity, recruitment of slow inhibitory factors, etc.) would have similar effects in terms of reduced efficiency in synaptic transmission.

Our model suggests a clear role for extracellular K^+ concentration as a mechanism for the initiation, but not the termination, of ictal events. This is consistent with observations in biological models which show that $[K^+]_o$ tends to increase rapidly at ictal onset, reaching a steady-state value early in the ictal event, even tapering off slightly well before the ictal event terminates (Heinemann et al., 1977; Avoli et al., 2002). This observation implies that it is unlikely that K^+ accumulation alone could account for both seizure onset and termination, e.g. from depolarization blocking of Na^+ channels (Fröhlich et al., 2008).

Conversely, evidence from intracellular recordings of pH have shown increasing acidification during ictal events (Xiong et al., 2000), reaching a minimum pH as the seizure terminates. This argues for the plausibility of acidosis as a correlate, if not the direct cause, of seizure termination. Our slow depression mechanism, while it does not attempt to model the physiological effects of acidosis, is consistent with the observed time course of changes in pH during ictal events.

We are not aware of any work which measures extracellular K^+ concentration during electrical stimulation *in vitro*. However, as described in Section 3.6, our model predicts that $[K^+]_o$ should be somewhat elevated during electrical stimulation.

A key problem in this area of research is fitting the many parameters used in the model. In this work, the data from the *in vitro* experiments was not directly used to tune any parameters, but only to perform the empirical comparisons. Alternatively, it may be possible to perform automatic parameter fitting in computational

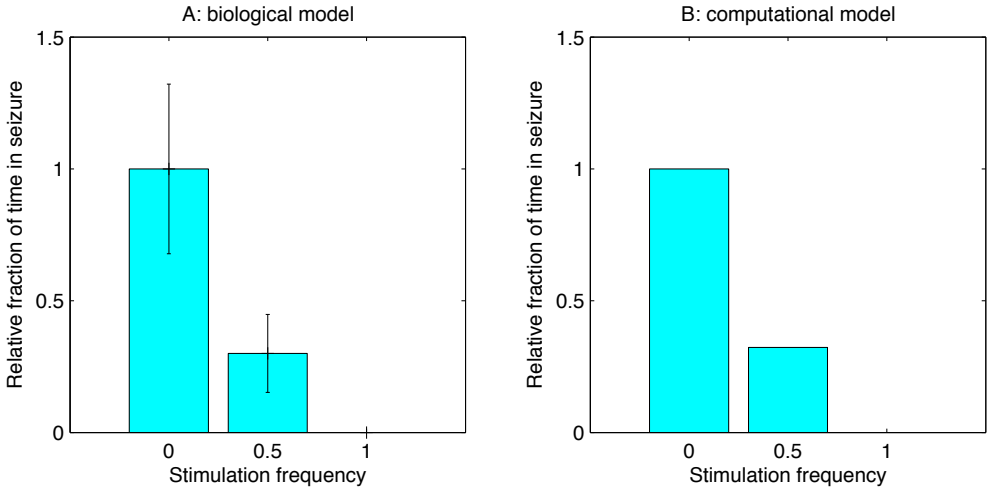

Figure 5: Effect of electrical stimulation on the relative percentage of time spent in seizure-like activity in A: the biological model and B: the computational model ($\Delta_Q = 0.00024$, $\tau_Q = 240$). Error bars are not shown for the computational model because the means are calculated using a single one-hour trial under each condition.

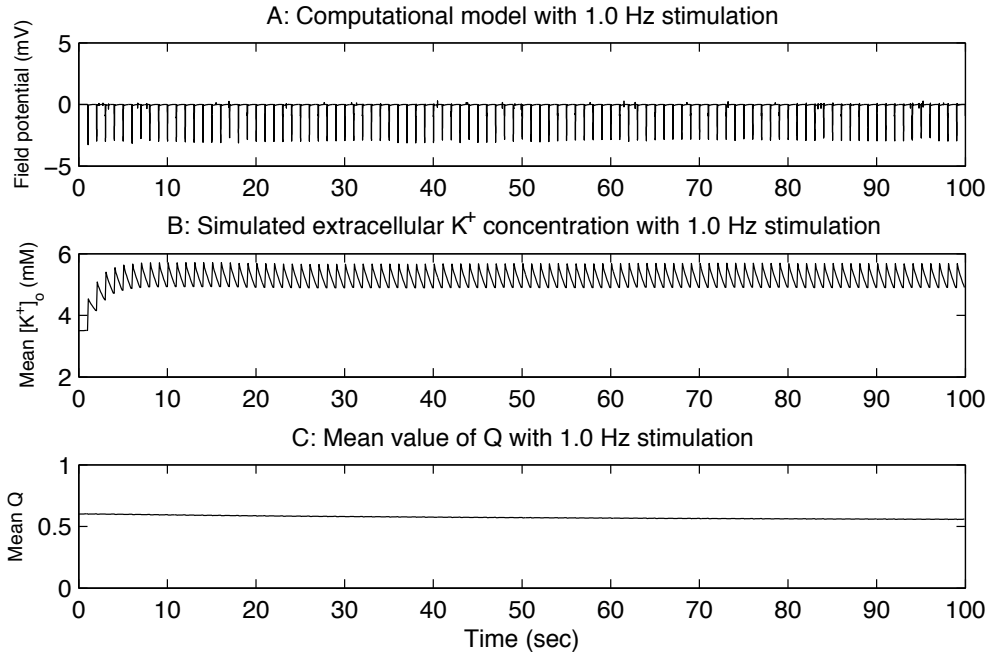

Figure 6: The computational model under the effects of stimulation at 1.0 Hz. A: The field potential trace of the model; B: The mean extracellular potassium concentration for the model under stimulation; C: The mean value of the slow depression variable Q. Only the first hundred seconds of the simulation is shown to illustrate the details of stimulation events; the model continues in this steady-state for the entire subsequent simulation.

models such as this. However, given that these models typically include a large number of free parameters, there are a number of potential pitfalls. Most obviously, the amount of both data and computation time required to perform such a fit may be prohibitively large. There is a tremendous risk of overfitting, which may lead to poor generalization in novel experimental conditions (e.g. predicting suppression in new stimulation frequencies). There is also a real possibility of the existence of numerous local minima, which would make the resulting optimization problem especially challenging.

Ultimately, the goal of this model is to provide an alternative source of data for the evaluation of responsive stimulation algorithms. Both the computational model and the *in vitro* biological model it mimics exhibit much greater regularity in seizure timing than is typically observed *in vivo*. However, the computational model does show substantial similarities in the timing of ictal events and the response to periodic pacing. The somewhat greater prevalence of preictal spiking in the computational model is of some concern, as this may provide an artificially large signal warning of the onset of an ictal event.

Acknowledgements

The authors gratefully acknowledge the assistance of G. Panuccio and M. Avoli, who collected the *in vitro* data and provided valuable comments on early versions of this manuscript. They also acknowledge the funding support of the Canadian Institutes of Health Research (CIHR) and the Natural Sciences and Engineering Research Council of Canada (NSERC).

References

Abbott, L. F., A., V. J., Sen, K., & Nelson, S. B. (1997). Synaptic depression and cortical gain control. *Science*, *275*, 221–224.

Avoli, M., D'Antuono, M., Louvel, J., Köhling, R., Biagini, G., Pumain, R., D'Arcangelo, G., & Tancredi, V. (2002). Network and pharmacological mechanisms leading to epileptiform synchronization in the limbic system in vitro. *Prog. Neurobiol.*, *68*, 167–207.

Bazhenov, M., Timofeev, I., Steriade, M., & Sejnowski, T. J. (2004). Potassium model for slow (2-3 Hz) in vivo neocortical paroxysmal oscillations. *J. Neurophysiol.*, *92*, 1116–1132.

Biswal, B., & Dasgupta, C. (2002). Neural network model for apparent deterministic chaos in spontaneously bursting hippocampal slices. *Phys. Rev. Lett.*, *88*, 088102.

Bush, K., & Pineau, J. (2009). Manifold embeddings for model-based reinforcement learning under partial observability. In Y. Bengio, D. Schuurmans, J. Lafferty, C. K. I. Williams, & A. Culotta (Eds.), *Advances in Neural Information Processing Systems 22* (pp. 189–197).

Cressman, J. R., Ullah, G., Ziburkus, J., Schiff, S. J., & Barreto, E. (2009). The influence of sodium and potassium dynamics on excitability, seizures, and the stability of persistent states: I. single neuron dynamics. *J. Comput. Neurosci.*, *26*, 159–170.

Crowder, J. M., Croucher, M. J., Bradford, H. F., & Collins, J. F. (1987). Excitatory amino acid receptors and depolarization-induced Ca^{2+} influx into hippocampal slices. *J. Neurochem.*, *48*, 1917–1924.

D'Arcangelo, G., Panuccio, G., Tancredi, V., & Avoli, M. (2005). Repetitive low-frequency stimulation reduces epileptiform synchronization in limbic neuronal networks. *Neurobiol. Dis.*, *19*, 119–128.

Dayan, P., & Abbott, L. F. (2001). *Theoretical Neuroscience: Computational and Mathematical Modeling of Neural Systems*. Cambridge, MA: MIT Press.

Destexhe, A., Mainen, Z. F., & Sejnowski, T. J. (1998). Kinetic models of synaptic transmission. In C. Koch, & I. Segev (Eds.), *Methods in neuronal modeling* (pp. 1–25).

Durand, D., & Bikson, M. (2001). Suppression and control of epileptiform activity by electrical stimulation: a review. *P. IEEE*, *89*, 1065–1082.

Franaszczuk, P. J., Kudela, P., & Bergey, G. K. (2003). External excitatory stimuli can terminate bursting in neural network models. *Epilepsy Res.*, *53*, 65–80.

Fröhlich, F., Bazhenov, M., Iragui-Madoz, V., & Sejnowski, T. J. (2008). Potassium dynamics in the epileptic cortex: new insights on an old topic. *The Neuroscientist*, *14*, 422–433.

Fröhlich, F., Sejnowski, T., & Bazhenov, M. (2010). Network bistability mediates spontaneous transitions between normal and pathological brain states. *J. Neurosci.*, *30*, 10734–10743.

Fujikawa, D. G., Kim, J. S., Daniels, A. H., Alcaraz, A. F., & Sohn, T. B. (1996). In vivo elevation of extracellular potassium in the rat amygdala increases extracellular glutamate and aspartate and damages neurons. *Neuroscience*, *74*, 695–706.

Golomb, D., & Amitai, Y. (1997). Propagating neuronal discharges in neocortical slices: computational and experimental study. *J. Neurophysiol.*, *78*, 1199–1211.

Golomb, D., Shedmi, A., Curtu, R., & Ermentrout, G. B. (2006). Persistent synchronized bursting activity in cortical tissues with low magnesium concentration: a modeling study. *J. Neurophysiol.*, *95*, 1049–1067.

Guez, A., Vincent, R. D., Avoli, M., & Pineau, J. (2008). Adaptive treatment of epilepsy via batch-mode reinforcement learning. In M. Goker, & K. Haigh (Eds.), *Proceedings of the 20th National Conference on Innovative Applications of Artificial Intelligence* (pp. 1671–1678). AAAI Press.

Heinemann, U., Lux, H. D., & Gutnick, M. J. (1977). Extracellular free calcium and potassium during paroxysmal activity in the cerebral cortex of the cat. *Exp. Brain Res.*, *27*, 237–243.

Hodgkin, A. L., & Huxley, A. F. (1952). A quantitative description of membrane current and its application to conduction and excitation in nerve. *J. Physiol.-London*, *117*, 500–544.

Jahr, C. E., & Stevens, C. F. (1990). A quantitative description of NMDA receptor-channel kinetic behavior. *J. Neurosci.*, *10*, 1830–1837.

Jensen, M. S., Azouz, R., & Yaari, Y. (1994). Variant firing patterns in rat hippocampal pyramidal cells modulated by extracellular potassium. *J. Neurophysiol.*, *71*, 831–839.

Jensen, M. S., Cherubini, E., & Yaari, Y. (1993). Opponent effects of potassium on $GABA_a$-mediated postsynaptic inhibition in the rat hippocampus. *J. Neurophysiol.*, *69*, 764–771.

Kager, H., Wadman, W. J., & Somjen, G. G. (2000). Simulated seizures and spreading depression in a neuron model incorporating interstitial space and ion concentrations. *J. Neurophysiol.*, *84*, 495–512.

Läuger, P. (1991). *Electrogenic ion pumps*. Distinguished lecture series of the Society of General Physiologists. Sunderland, MA: Sinauer.

Löscher, W., & Köhling, R. (2010). Functional, metabolic, and synaptic changes after seizures as potential targets for antiepileptic therapy. *Epilepsy Behav.*, *19*, 105–113.

Netoff, T. I., Clewley, R., Arno, S., Keck, T., & White, J. A. (2004). Epilepsy in small-world networks. *J. Neurosci.*, *24*, 8075–8083.

Ohayon, E., Kwan, H., Burnham, W., Suffczynski, P., & Kalitzin, S. (2004). Emergent complex patterns in autonomous distributed systems: mechanisms for attention recovery and relation to models of clinical epilepsy. In *2004 IEEE International Conference on Systems Man and Cybernetics* (pp. 2066–2072). volume 2.

Perreault, P., & Avoli, M. (1991). Physiology and pharmacology of epileptiform activity induced by 4-aminopyridine in rat hippocampal slices. *J. Neurophysiol.*, *65*, 771–785.

Poolos, N. P., & Kocsis, J. D. (1990). Elevated extracellular potassium concentration enhances synaptic activation of N-methyl-D-aspartate receptors in hippocampus. *Brain Res.*, *508*, 7–12.

Rivera, C., Voipio, J., Thomas-Crusells, J., Li, H., Emri, Z., Sipila, S., Payne, J., Minichiello, L., Saarma, M., & Kaila, K. (2004). Mechanism of activity-dependent downregulation of the neuron-specific K-Cl cotransporter KCC2. *Journal of Neuroscience*, *24*, 4683–4691.

Su, H., Alroy, G., Kirson, E., & Yaari, Y. (2001). Extracellular calcium modulates persistent sodium current-dependent burst-firing in hippocampal pyramidal neurons. *J. Neurosci.*, *21*, 4173–4182.

Suffczynski, P., Kalitzin, S., & Lopes Da Silva, F. H. (2004). Dynamics of non-convulsive epileptic phenomena modeled by a bistable neuronal network. *Neuroscience*, *126*, 467–484.

Sun, F. T., Morrell, M. J., & Wharen, R. E. (2008). Responsive cortical stimulation for the treatment of epilepsy. *Neurotherapeutics*, *5*, 68–74.

Tateno, K., Hayashi, H., & Ishizuka, S. (1998). Complexity of spatiotemporal activity of a neural network model which depends on the degree of synchronization. *Neural Networks*, *11*, 985–1003.

Traub, R. D., Bibbig, R., Piechotta, A., Draguhn, R., & Schmitz, D. (2001). Synaptic and nonsynaptic contributions to giant IPSPs and ectopic spikes induced by 4-aminopyridine in the hippocampus in vitro. *J. Neurophysiol.*, *85*, 1246–1256.

Traub, R. D., Colling, S. B., & Jefferys, J. G. (1995). Cellular mechanisms of 4-aminopyridine-induced synchronized after-discharges in the rat hippocampal slice. *J. Physiol.-London*, *489 (Pt 1)*, 127–140.

Traub, R. D., Contreras, D., Cunningham, M. O., Murray, H., LeBeau, F. E. N., Roopun, A., Bibbig, A., Wilent, W. B., Higley, M. J., & Whittington, M. A. (2005). Single-column thalamocortical network model exhibiting gamma oscillations, sleep spindles, and epileptogenic bursts. *J. Neurophysiol.*, *93*, 2194–2232.

Ullah, G., Cressman, J. R., Barreto, E., & Schiff, S. J. (2009). The influence of sodium and potassium dynamics on excitability, seizures, and the stability of persistent states: II. network and glial dynamics. *J. Comput. Neurosci.*, *26*, 171–183.

Uthman, B. M., Reichl, A. M., Dean, J. C., Eisenschenk, S., Gilmore, R., Reid, S. A., Roper, S. N., & Wilder, B. J. (2004). Effectiveness of vagus nerve stimulation in epilepsy patients: A 12 year observation. *Neurology*, *63*, 1124–1126.

Wang, X. J., & Buzsáki, G. (1996). Gamma oscillation by synaptic inhibition in a hippocampal interneuronal network model. *J. Neurosci.*, *16*, 6402–6413.

Xiong, Z. Q., Saggau, P., & Stringer, J. L. (2000). Activity-dependent intracellular acidification correlates with the duration of seizure activity. *J. Neurosci.*, *20*, 1290–1296.

Ziemann, A. E., Schnizler, M. K., Albert, G. W., Severson, M. A., Howard, M. A., Welsh, M. J., & Wemmie, J. A. (2008). Seizure termination by acidosis depends on ASIC1a. *Nat. Neurosci.*, *11*, 816–822.